Modeling the hot deformation behavior of micro-alloyed steel in the single and two-phase fields

Modeling the hot deformation behavior of micro-alloyed steel in the single and two-phase fields

S S Sharifi[1*], R H Buzolin[1,4], S Bakhtiari[1,2], M Gontijo[1,3], C Sommitsch[1] and M C Poletti[1,4]

[1] Institute of Materials Science, Joining and Forming at Graz University of Technology, Kopernikusgasse 24/I, 8010, Graz, Austria
[2] K1-MET GmbH, 4020 Linz, Austria
[3] Andritz AG, Stattegger Straße 18, 8045 Graz, Austria
[4] Christian Doppler Laboratory for Design of High-Performance Alloys by Thermomechanical Processing, Kopernikusgasse 24, 8010, Graz, Austria

Abstract. Continuous casting is a well-established process to produce steel slabs. However, the surfaces of the slabs may crack during processing. The occurrence of cracks is related to different phenomena, i.e., ferrite formation, presence of precipitates, and microstructural modifications during manufacturing processing. In the present work, we developed a physically based mesoscale model to describe the plastic deformation of micro-alloyed steel in the single and two-phase fields, as well as the microstructure evolution. We implemented a dislocation density-based constitutive model to calculate the strain hardening and the stress softening produced by dynamic recovery using the Kocks-Mecking (KM) formalism for the austenite and ferrite. We coupled the KM model with the Johnson-Mehl-Avrami-Kolmogorov model to consider the dynamic recrystallization of the austenitic phase. The nucleation and growth of the recrystallized grains, driven by the stored energy, compete with the annihilation of dislocations due to dynamic recovery. In the two-phase domain, the iso-work condition for the load partition is implemented. We calculated the ferrite volume fraction by fitting the data obtained using JmatPro software. Moreover, an Arrhenius-type equation correlates the yield stress to the Zener-Hollomon parameter. We validated the model with isothermal uniaxial compression tests of microalloyed steel over the temperature range of 650 °C-1100 °C and strain rates of 10^{-2} s^{-1} and 10^{-3} s^{-1} using a Gleeble® 3800 thermomechanical simulator.

Keywords: plastic deformation, dynamic recovery, dynamic recrystallization, mesoscale modeling, micro-alloyed steels

1 Introduction

Continuous casting process is largely used to produce slabs of steels . Sometimes, slabs can present superficial cracks due to the thermomechanical stresses that arise during the continuous casting process, especially between 700 °C and 1000 °C [1,2]. Steels undergo plastic deformation in the temperature range of 700 °C–1000 °C after solidification [2,3]. In this temperature range, it has been reported that the material becomes brittle during deformation, leading to surface crack initiation [3–5]. Various factors, for instance, the presence of proeutectoid ferrite film, precipitates, and microstructural modification during hot deformation influence the ductility behavior [2,3].

Chemical composition significantly impacts the hot ductility behavior of steels. Vedani et al. observed that damage increases as temperature increases from 850 °C to 950 °C for the same strain level [1]. They showed that the distribution of fine precipitates at grain boundaries promotes crack nucleation, enhancing hot-crack damage. They reported that Nb reduces the hot crack resistance in the studied steel grades, while Ti improves the hot ductility. Zheng et al. showed that Nb reduces the hot ductility when increasing the temperature from 650 °C to 850 °C [6]. Moreover, they reported that the addition of B improves the hot ductility in Nb-containing steels. They attributed this to the fact that Nb promotes ferrite transformation at a higher temperature, while B retards the ferrite transformation. Therefore, Nb-containing micro-alloyed steels show lower hot ductility due to a higher amount of ferrite films at grain boundaries than those containing B. However, the hot ductility of Nb-B steels is still lower than that of non-alloyed steels [6]. Gontijo et al. studied the influence of precipitates

and ferrite formation kinetics at grain boundaries on the hot ductility of micro-alloyed steels [7]. They concluded that the addition of B and Ti improves the hot ductility of the studied alloys by forming TiN and BN instead of AlN, which is a more detrimental precipitate.

The microstructure evolution of steels during processing is complex. The microstructure changes are dictated by the occurrence of hardening and restoration mechanisms. These mechanisms are affected by the thermomechanical parameters, such as temperature, strain rate, and strain, as well as some physical characteristics of the material [2,4,6]. The effect of the amount of ferrite on hot ductility has been largely reported [6,8,9]. During hot deformation, the strain concentrates on the softer phase (ferrite film at the grain boundaries), causing the initiation and crack propagation [9]. Gontijo et al. investigated the effect of deformation conditions on the fracture behavior of a micro-alloyed steel [2]. They reported that at high strain rates, the time for ferrite formation during deformation is not enough and that voids also do not have enough time to nucleate and grow. However, the influence of simultaneous dynamic restoration mechanisms was not discussed.

In recent years, significant efforts have been made by various research groups to develop constitutive models that accurately describe the flow behavior of metals and alloys [9–13]. These models play a crucial role in predicting and understanding the microstructure evolution during hot deformation, particularly in the case of low alloyed steels. The models are mainly composed of three categories, including phenomenological models, physically based models, and artificial neural network models. Among phenomenological constitutive models, the Arrhenius hyperbolic-sine equation is the most widely used. Mirzadeh et al. developed constitutive equations to describe the flow behavior of austenite [12]. They determined the apparent deformation activation energy and material constants by employing three expressions of the Zener-Hollomon parameter: the power law, the exponential law, and the hyperbolic sine law. However, while these phenomenologically based constitutive equations effectively capture the hot working characteristics of steels, the underlying deformation mechanisms lack clear physical interpretations. In contrast, physically based models, such as the Kocks-Mecking model [14], treat dislocation density as an internal variable that represents the microstructural state of materials. This model finds widespread application in describing the high-temperature deformation behaviors of various alloys. By combining dislocation density theory with dynamic recrystallization mechanisms, researchers have developed physically based constitutive models that effectively describe the strain hardening, dynamic recovery, and dynamic recrystallization behaviors of steels. One notable attempt by Zurob et al. involves the coupling of recovery, recrystallization, and precipitation phenomena into a single model [15]. This integrated approach aimed to provide a comprehensive understanding of the complex microstructure evolution during hot deformation. However, while the model successfully described the interaction between these phenomena, its fitting parameters were based on phenomenological assumptions specific to a particular material. Furthermore, the model did not account for the influence of temperature and strain rate on the underlying softening mechanisms. In a separate study, Timoshenkov et al. developed a physically based model to describe the dynamic recrystallization of C-Mn micro-alloyed steel using a two-dimensional cellular automaton model [16]. While their work provided valuable insights into the recrystallization process, it focused exclusively on the single-phase domain, overlooking the microstructural evolution in the two-phase domain. This gap in knowledge is significant as low alloyed steels commonly exhibit a two-phase microstructure comprising both austenite and ferrite phases during the manufacturing process, such as continuous casting.

Most of the existing works explain ductility degradation during steel processing based on experimental observations. However, any modification in the chemical composition or the processing parameters would require a complete analysis of the hot ductility behavior. Therefore, there is a need for models that can predict the microstructure evolution during deformation and its correlation with damage. This paper presents a physically based model that effectively correlates flow stresses with the microstructure of low alloyed steels within the temperature range associated with their low ductility. Our approach involves the development of a microstructural constitutive model that considers the load partition between austenite and ferrite. We validated the model with hot compression tests and metallography observations. The developed model provides a basis for further investigations into the mechanical properties of low alloyed steels during various manufacturing processes, particularly continuous casting.

2 Materials and experiments

Table 1 gives the chemical composition of the investigated micro-alloyed steel. We performed hot compression tests to obtain the flow curves and metallography for the microstructure. The samples were

machined from the slab produced by continuous casting, with a diameter of 10 mm and 15 mm long, and with the long axis parallel to the direction of casting.

Table 1. Chemical composition of the studied micro-alloyed steel [wt%].

C	Cr	Mn	Al	N	Ni	Si	S	P	Nb	Ti	B	Fe
0.079	0.28	1.67	0.051	0.0052	0.028	0.124	0.0051	0.013	0.003	0.0014	0.0002	bal.

We compressed the cylindrical samples at temperatures between 650 °C and 1100 °C using a Gleeble® 3800 machine. Before compression, we heated the samples up to 1200 °C at 5 °C/s, soaked for 360 seconds, cooled to the deformation temperature at 1 °C/s, and held for 15 s before deformation. The compression proceeded at strain rates of 10^{-2} s^{-1} and 10^{-3} s^{-1}. Two S-type thermocouples were welded on the surface of the samples to measure the temperature. One thermocouple was located at the centre of the sample to control the temperature, while the other thermocouple was attached at the edge to measure the longitudinal temperature gradient developed before the deformation. We used an Ar atmosphere to avoid oxidation. After deformation, the samples were water quenched to preserve the microstructure for posterior characterization. Moreover, three additional samples of 750 °C, 900 °C, and 1100 °C are quenched right before the start of deformation to obtain the initial microstructure of the alloy at this point. The microstructure characterization proceeded after metallographic preparation. We cut the samples in the direction of deformation, embedded them in resin, ground them with SiC papers up to P1200, and polished them. The polishment was with an alumina suspension with 1μm of particle size for 5 minutes, and with a colloidal silica suspension for 10 minutes. We used a saturated aqueous solution of picric acid for 6-10 minutes to identify the prior austenite grain boundaries. Finally, we used a with a Zeiss Observer Z1m optical microscope (Carl Zeiss, Jena, Germany) to observe the microstructure. The Heyn Lineal Intercept method (ASTM E112-2010) implemented in the ImageJ software allowed us to determine the grain size out of three images of each temperature. The samples heat treated at 750 °C, 900 °C, and 1100 °C with no deformation present similar austenite grain sizes since they experienced the same austenitization temperature. The measured initial average austenite grain size was of 100 μm.

3 Modeling setup

The model describes the microstructure and the flow stress evolutions in both the single austenite and the austenite/ferrite fields. The model is given in equations 1 to 19. It considers the strain rate partitioning between the phases and the dislocation density evolution. In high SFE materials, like ferrite, dislocations glide with ease. Therefore, the dislocation density increases in the early stages of deformation. With further straining, the rate of strain hardening gradually decreases due to the dynamic annihilation of dislocations, leading to a steady-state flow. Such behavior represents dynamic recovery (DRV) as the main restoration mechanism characterized by flow curves that reach a stress plateau when the rates of DRV and strain hardening come into balance [17,18]. Low SFE materials, such as austenite, tend to form stacking faults from perfect dislocations that have difficult gliding and cross-slipping. At the early stages of deformation, a high level of dislocation density provides a sufficient driving force for nucleating new grains, followed by growth, i.e., dynamic recrystallization (DRX) [16–18].

Equation (1) gives the yield stress, $\sigma_{y,x}$ [19]. The subscript x denotes the austenite (γ) and ferrite (α) phases. The Zener-Hollomon parameter, Z, is correlated to the temperature T and strain rate $\dot{\varepsilon}$ through equation (2). The activation energy, Q_x, and the parameters A, a_x, n_x, are listed in appendix A, Table A1. R is the universal constant of gases. Furthermore, we determined the strain rate in each phase as proposed by Bouaziz [20]. We consider the iso-work condition, meaning that the amount of mechanical work increment in each phase as the same. The load partitioning between ferrite and austenite is described according to equations (16) and (17). Thereafter, equations (18) and (19) give the strain rate in each phase. We calculated the austenite phase fraction fγ and the ferrite phase fraction f_α, using CCT and TTT diagrams produced by JMatPro® software. The overall phase fraction is the sum of the fractions of the ferrite formed during cooling and the ferrite formed during deformation. The former is determined using a CCT diagram, and the latter using TTT diagrams at the respective deformation temperature. The represented microstructure is composed of dislocations and grain boundaries. The immobile dislocation density, ρ_i, stands for the dislocations that are immobilized, while ρ_m represents the mobile dislocation density moving short-range distances. We assume that the mobile dislocation density remains constant if the strain rate is kept constant during the deformation.

The developed model considers that the overall stress, σ, can be calculated as the sum of the contributions of athermal σ_{ath} and thermal σ_{th} stresses. The thermal stress is given by equation (3). The initial athermal

stress is calculated based on the initial immobile and mobile dislocation densities given in appendix A Table A1. Equation (4) gives the athermal stress that follows the Taylor equation [14]. In equation (4), μ_x is the temperature-dependent shear modulus, M is the Taylor factor, a is the stress constant, and b is the burgers vector. Equation (5) represents the evolution rate of immobile dislocation density in each phase as proposed by Kocks-Mecking [14,18] . Equations (6) and (7) give the dependency of the work hardening $h_{1,x}$ and recovery $h_{2,x}$ coefficients on the temperature and strain rate. The fitting parameters $h_{01,x}$, $m_{h1,x}$, $Q_{h1,x}$, $h_{02,x}$, $m_{h2,x}$, and $Q_{h2,x}$ are listed in appendix A.

During plastic deformation of austenite, dislocation density increases until it reaches a critical value for the onset of DRX identified as the critical strain, ε_{cr}. This critical strain can be experimentally correlated to the peak strain, ε_p through the $\varepsilon_{cr} = B\varepsilon_p$ relationship (where B is a constant between 0.5 and 0.8) [17]. Once the grains reach the critical dislocation density, the nucleation occurs at prior austenitic grain boundaries. Equation (8) correlates the nucleation rate, $\check{N}$, to the deformation temperature and grain boundary energy. In this equation $Q_n \sim \gamma_{gb}b^2$ is the activation energy, N_0 is a pre-exponential factor and k_B is the Boltzmann constant.

After nucleation, the grains grow by grain boundary migration with a velocity v given by the applied pressure on the boundary, P, multiplied by the mobility M_g of the grain boundary M_g. Equation (9) defines the grain-boundary mobility in which M_0 is a pre-exponential mobility factor and Q_{bd} is the boundary-diffusion activation energy [16]. The pressure on the boundary, P, is represented in equation (10). Moreover, in equation (11) the size of the nucleus is correlated with the total dislocation density and the initial grain size Φ_0, where κ is a constant of the material. We assume that the velocity of the recrystallized grain reduces the velocity of the deforming grain by nucleating new grains over time (equation (12)). Δg_{drx} is the change in the size of recrystallized grain after nucleation ($\delta_{nuclei} - g_{drx}$). In this way, the model updates the size of recrystallized grain in each step.

The recrystallization fraction X(t) is a function of g_{drx} and the number of nuclei N as shown in equation (13) (q is a constant). The recrystallization reduces the dislocation density and therefore, the stress values. The average dislocation density ρ_{ave} takes into account the dislocation density reduction due to the softening through DRX (equation (14)) towards reaching the dislocation density at the steady state $\rho_{ss,drx}$. Finally, the model calculates the average grain sizes considering recrystallized and non-recrystallized grain populations through equation (15).

$$\sigma_x = \frac{1}{a_x} ln\left\{\left(\frac{Z}{A}\right)^{\frac{1}{n_x}} + \left[\left(\frac{Z}{A}\right)^{\frac{2}{n_x}} + 1\right]^{0.5}\right\}, \text{x} = \alpha, \gamma \quad (1)$$

$$Z = \dot{\varepsilon}_x \, exp\left(\frac{Q_x}{RT}\right), \quad \text{x} = \alpha, \gamma \quad (2)$$

$$\sigma^0_{th,x} = \sigma_{y,x} - \sigma^0_{ath,x}, \quad \text{x} = \alpha, \gamma \quad (3)$$

$$\sigma_{ath,x} = M_x a_x \mu_x b_x \sqrt{\rho_{i,x} + \rho_{m,x}}, \text{x} = \alpha, \gamma \quad (4)$$

$$\frac{d\rho_{i,x}}{dt} = \dot{\varepsilon}\left(h_{1,x}\sqrt{\rho_{i,x} + \rho_{m,x}} - h_{2,x}(\rho_{i,x} + \rho_{m,x})\right), \quad \text{x} = \alpha, \gamma \quad (5)$$

$$h_{1,x} = h_{01,x}\dot{\varepsilon}^{m_{h1,x}} exp\left(\frac{m_{h1,x}.Q_{h1,x}}{RT}\right) \quad (6)$$

$$h_{2,x} = h_{02,x}\dot{\varepsilon}^{-m_{h2,x}} exp\left(\frac{-m_{h2,x}.Q_{h2,x}}{RT}\right) \quad (7)$$

$$\check{N} = N_0 \exp\left(\frac{-Q_n}{k_B T}\right) \quad (8)$$

$$M_g = M_0 \exp\left(\frac{Q_{bd}}{RT}\right) \quad (9)$$

$$P = 0.5\mu b^2(\rho_i + \rho_m) \quad (10)$$

$$\delta_{nuclei} = \frac{1}{\kappa\sqrt{\rho_i + \rho_m} + \frac{1}{\Phi_0}} \quad (11)$$

$$v_{drx} = v_g + \left(\frac{\Delta g_{drx}}{dt}\right) \quad (12)$$

$$X(t) = 1 - \exp(-qNg^3_{drx}) \quad (13)$$

$$\rho_{ave} = (1 - X)(\rho_{m,\gamma} + \rho_{i,\gamma}) + X\rho_{ss,drx} \quad (14)$$

$$\Phi_{ave} = \Phi_0[1 - X(t)] + \Phi_{drx}.X(t) \quad (15)$$

$$\sigma_\gamma \dot{\varepsilon}_\gamma = \sigma_\alpha \dot{\varepsilon}_\alpha \quad (16)$$

$$\sigma_T = (1 - f_\gamma)\sigma_\alpha + f_\gamma \sigma_\gamma \quad (17)$$

$$\dot{\varepsilon}_\gamma = \frac{\dot{\varepsilon}}{f_\alpha(\frac{\sigma_\gamma}{\sigma_\alpha}) + 1 - f_\alpha} \quad (18)$$

$$\dot{\varepsilon}_\alpha = \frac{\dot{\varepsilon}\,(\frac{\sigma_\gamma}{\sigma_\alpha})}{f_\alpha(\frac{\sigma_\gamma}{\sigma_\alpha}) + 1 - f_\alpha} \quad (19)$$

4 Results and discussion

4.1 Flow curves

Figure 1 compares the experimental and simulated flow curves of the studied steel under different deformation conditions. The flow curves show three distinct regimes. At the early stages of the deformation, strain hardening predominates over softening and the dislocation density increases. With further straining, dislocations annihilation (DRV) or DRX softens the material. Finally, the steady-state regime is reached when the strain hardening is counterbalanced by dynamic softening [17]. However, the peak stress becomes less prominent as the temperature decreases or the strain rate increases. This observation can be attributed to the effect of these factors on the occurrence of DRX. With increasing deformation temperature, the driving force for the nucleation of recrystallized grains also increases, promoting the occurrence of DRX [12]. A similar trend is observed at lower deformation rates, where the extended time available favors the activation of softening mechanisms (**Figure 1**(a) and (b)). The flow curves also show that the flow stress decreases as the deformation temperature increases or the strain rate decreases. The drop in flow stress with increasing deformation temperature can be attributed to the enhanced rate of restoration processes and the reduction in the strain hardening rate [11,21].

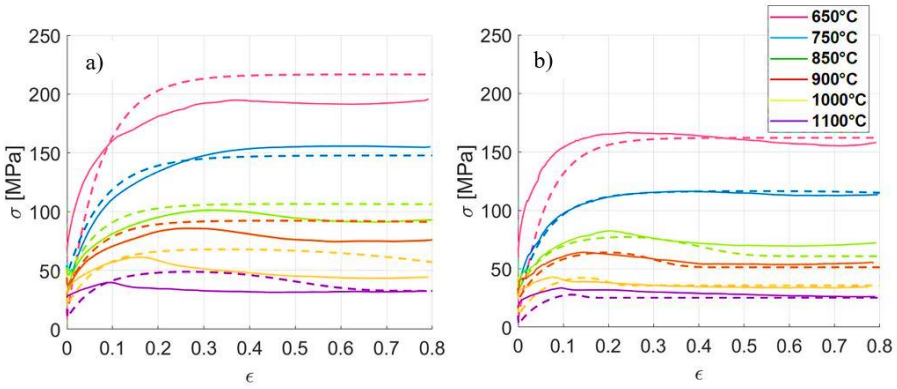

Figure 1. Modelled (dashed lines) and experimental (solid lines) flow curves at different temperatures and strain rates: a) 0.01 s^{-1} and b) 0.001 s^{-1}.

4.2 Dislocation density

The current model describes dislocation density evolution during plastic deformation. **Figure 2** shows the evolution of the immobile dislocation density (dotted curves) and average dislocation density (solid curves) under different deformation conditions Initially, during the early stages of deformation, the dislocation density increases sharply due to dislocation multiplication. As the deformation progresses, the dislocations annihilate, reducing the work hardening [17,18]. This process involves a competition between work hardening and dynamic restoration, which continues until a strain is reached where the multiplication and annihilation of dislocations reach equilibrium, resulting in a steady state [18,22]. The dislocation density evolution is influenced by thermomechanical conditions such as deformation temperature and strain rate. The dislocation density roughly increases with decreasing deformation temperature or increasing strain rate. In the early stages of deformation, the dislocation density shows a rapid increase. However, as the deformation progresses, the accumulation rate of dislocation density gradually decreases due to the occurrence of dislocation annihilation (DRV). Once a dynamic equilibrium between strain hardening and dynamic recovery is achieved, the dislocation density stabilizes at a relatively constant value. Conversely, at higher temperatures and lower strain rates, the formation of DRX nuclei becomes easier, thereby enhancing the kinetics of DRX. Additionally, the mobility of grain boundaries increases with rising deformation temperature, leading to an accelerated rate of DRX. Consequently, the dislocation density decreases [18,23,24].

The model successfully reproduces the characteristic softening peaks associated with the dynamic recrystallization of austenite. As DRX occurs, the material undergoes softening, resulting in a decrease in the average dislocation density until it reaches a plateau in a fully recrystallized state ($\rho_{ss,drx}$). The occurrence of DRX is more rapid at higher temperatures and lower strain rates, and it completes at smaller strains (**Figure 2** (a) and (b)).

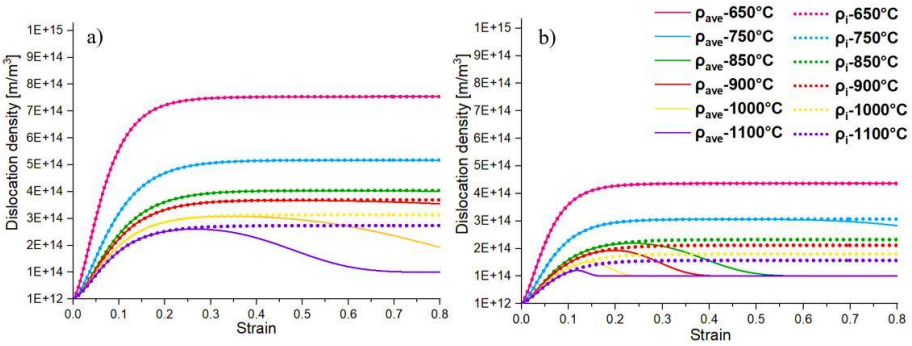

Figure 2. Immobile dislocation density (dotted) and average dislocation density (solid) evolution at different temperatures and strain rates: a) 0.01 s^{-1}, and b) 0.001 s^{-1}.

4.3Microstructure evolution

The model provides recrystallization grade under different deformation conditions (**Figure 3**). Higher temperatures and lower strain rates promote a more pronounced DRX phenomenon in steels [18,22]. Elevated temperatures provide the necessary thermal energy for the nucleation and growth of recrystallized grains, thereby facilitating the occurrence of DRX. Higher temperatures reduce the activation energy barriers for grain boundary migration, leading to enhanced mobility and facilitated grain boundary movement necessary for recrystallization. As a result, the DRX grade tends to be higher at these temperatures [17,24]. In contrast, lower temperatures and higher strain rates restrict the mobility and interaction of dislocations, hindering the DRX. The reduced thermal energy limits the recrystallization process, resulting in a lower DRX grade. Moreover, higher strain rates provide limited time for the necessary nucleation and growth of recrystallized grains (**Figure** 3 (a) and (b)). The model replicates the low DRX grade of austenite in the two-phase field (below 830 °C) and the increment of DRX grade with the temperature and the inverse of the strain rate. **Figure 4** shows the experimental and modeled average grain size at the end of the deformation. At 750 °C, and at both strain rates, the average grain size does not change since the amount of DRX is insignificant.

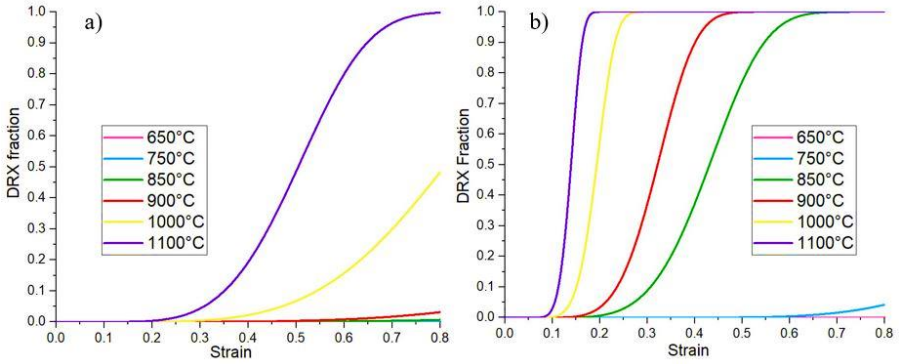

Figure 3. DRX evolution at different temperatures and strain rates: a) 0.01 s^{-1}, and b) 0.001 s^{-1}.

The DRX modifies the microstructure as temperature increases and strain rate decreases. In such conditions, there is sufficient time for energy accumulation, and the temperature is high enough to provide the driving force for recrystallized grains to nucleate and modify the microstructure [18]. However, the fraction and size of these grains decrease with increasing strain rate and decreasing temperature (**Figure 3**a,b, and **Figure 4**). In **Figure 4**, high standard deviation, e.g., at 1000 °C and a strain rate of 10^{-2} s^{-1}, is attributed to the heterogeneous microstructure of a partially recrystallized matrix (**Figure 5**b.1). After complete recrystallization, the average grain size remains constant, which is equal to the size of recrystallized grain at steady state. Although the current model does not consider multiple DRX cycles, with further deformation of a fully recrystallized microstructure, the dislocation density increases again, providing enough driving force for posterior DRX. In

these conditions, the competition between strain hardening and restoration processes in each cycle results in oscillations in the flow curve.

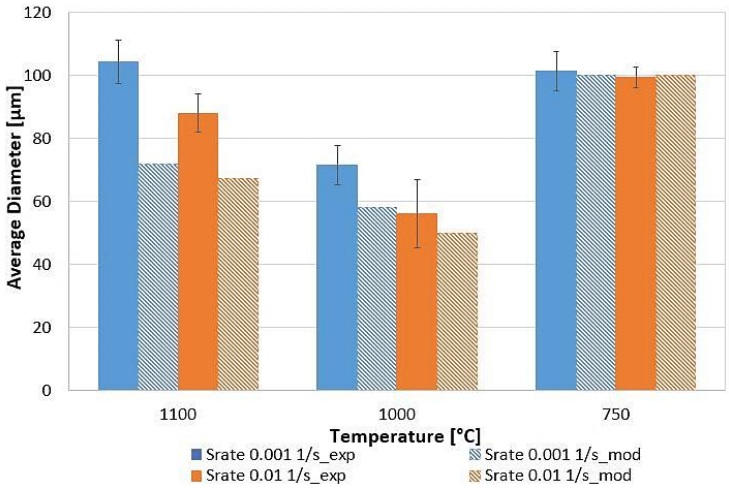

Figure 4. Modelled (dashed bars) and experimental (solid bars) average grain size at different temperatures and strain rates up to a strain of 0.8.

Figure 5 represents the correlation of the model with the optical microscopy images of the deformed samples at the final strain (0.8). At the lowest temperature, the DRX fraction is trivial since the temperature is not high enough to promote DRX in austenite. Therefore, the microstructure consists of elongated austenite grains covered by ferrite along the grain boundaries (**Figure 5**a.1, a.2). By increasing the temperature and decreasing the strain rate, the material recrystallizes leading to an equiaxed microstructure (**Figure 5**b, and c). The size of recrystallized grains increase with increasing the temperature and decreasing the deformation rate.

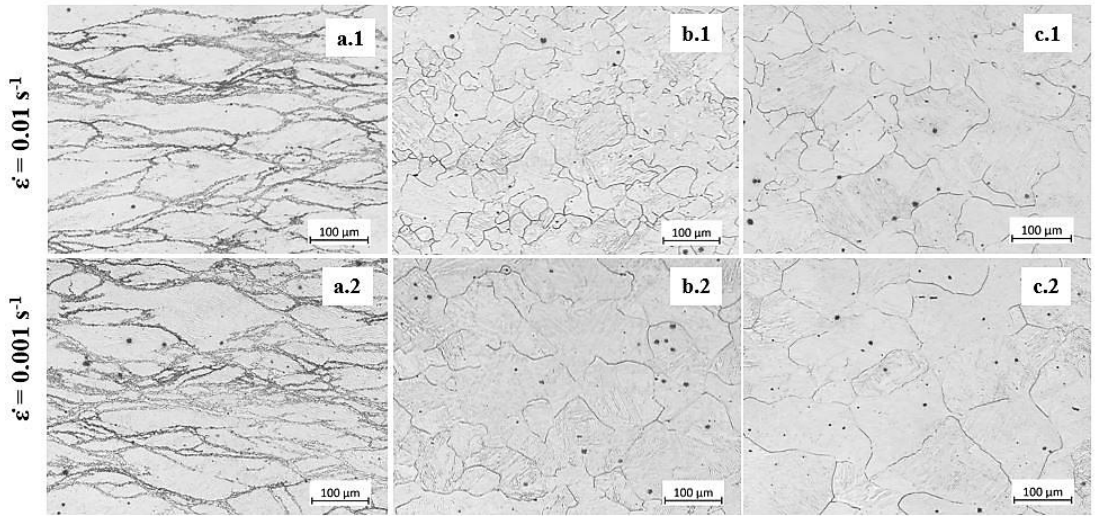

Figure 5. Optical micrographs of the samples deformed at different temperatures at ε = 0.8: a.1,2) 750 °C, b.1,2) 1000 °C, c.1,2) 1100 °C.

5 Summary and Conclusions

This study highlights the significant impact of microstructure modification on the mechanical properties, particularly hot ductility, of steel in the manufacturing process. This work provides a basis for tailoring and gaining insights into the microstructural evolution of micro-alloyed steels during hot deformation. A mean field flow stress model was developed, incorporating dislocation density as an internal variable, to analyze the deformation behavior of micro-alloyed steel at moderate and elevated temperatures. We implemented the yield

stress dependency on the thermomechanical processing conditions in the model. We employed the mixture law of recrystallized and unrecrystallized phases, along with the iso-work law for load partitioning between phases in the model. The knowledge obtained through this model is then used to describe the failure behavior of micro-alloyed steel during hot working, with a focus on the ferrite phase fraction and microstructural modifications that occur during hot deformation.

The results allow the following conclusions:

i. At lower temperatures, flow stresses initially increase during the first stage of plastic deformation, followed by a plateau when work hardening and dynamic recovery reach a balance at large strains.
ii. The flow curves exhibit a distinct peak associated with dynamic recrystallization (DRX) at higher temperatures and lower deformation rates.
iii. Lower temperatures and higher strain rates hinder DRX due to insufficient driving force and limited time for the nucleation of new recrystallized grains, respectively.
iv. The size of dynamically recrystallized grains after complete DRX primarily depends on the deformation temperature and strain rate. As the strain rate increases and the temperature decreases, the fraction and size of recrystallized grains decrease.
v. Apart from the formation of ferrite films along austenite grain boundaries, the microstructural changes induced by recrystallization-driven strain also impact the mechanical properties, such as hot ductility, of microalloyed steels. Increasing temperature facilitates DRX occurrence and, therefore, can improve the mechanical response.

Disclosure statement

No potential conflict of interest was reported by the author(s).

Data availability

Data will be made available on request.

Acknowledgments

The authors gratefully acknowledge the funding support of K1-MET GmbH. The research program of the K1-MET competence center is supported by COMET (Competence Center for Excellent Technologies), the Austrian program for competence centers. COMET is funded by the Federal Ministry for Climate Action, Environment, Energy, Mobility, Innovation and Technology, the Federal Ministry for Digital and Economic Affairs, the provinces of Upper Austria, Tyrol, and Styria, and the Styrian Business Promotion Agency (SFG). Additionally, the authors would like to extend their gratitude to Voestalpine Stahl GmbH for providing the samples for this research. RHB and MCP foster the Christian Doppler Laboratory for Design of High-Performance Alloys by Thermomechanical Processing with the support of the Christian Doppler Society. The authors are also grateful to E. Shahriari for providing a fitting parameter optimizer model. Open access funding by the Graz University of Technology is also acknowledged.

Appendix A

Table A1. Parameters, constants and internal variables used in this work

	Nomenclature [unit]	Ferrite	Austenite		Nomenclature	Ferrite	Austenite
b	Burgers vector [nm]	0.25	0.254	h_{01}	Initial value hardening coefficient [1/m]	35 x10^7	42.1 x10^7
α	Stress constant [-]	0.3	0.3	Q_{h1}	Activation energy for h_1 [kJ/mol]	5.18E3	5E3
M	Taylor factor [-]	3	3.1	m_{h1}	Strain rate sensitivity for h_1	0.055	0.05
ν	Poisson coefficient [a]	0.290+4E-5T	0.293+6E-5T	h_{02}	Initial value recovery coefficient	40	35
μ	Shear modulus [GPa] [a]	$\frac{(221.66-0.107T)}{(2.578+8E-5T)}$	$\frac{(206.4-0.1012T)}{(2.586+1.2E-4T)}$	Q_{h2}	Activation energy for h_2 [J/mol]	4.94E3	5.1E3
k_B	Boltzmann constant [J/K]	1.38x10^{-23}	1.38x10^{-23}	m_{h2}	Strain rate sensitivity for h_2	0.07	0.073
γ_g	HAGB energy [J/m^2]	-	0.6	M_0	Pre-exponential mobility factor [m^4/J/s]	-	0.15

N_0	Constant [-]	-	$7x10^{-5}$	Q_{bd}	Boundary-diffusion activation energy[kJ/mol]	-	135.1
κ	Nuclei size constant [-]	-	0.001	ϕ_0	Initial average grain diameter [μm]	-	100
f_i	Phase volume fraction [a]	$f(T,\dot{\varepsilon})$	$f(T,\dot{\varepsilon})$	Q_y	Activation energy in Z equation [kJ/mol]	670.3	389.9
A	Constant in yield stress	$1.47x10^{14}$	$4.43x10^{11}$	n_{ys}	Parameter in yield stress calculation	1.87	3.587
ρ_i^0	Initial immobile dislocation density [m^{-2}]	$1x10^{12}$	$1x10^{12}$	α_{ys}	Parameter in yield stress calculation [MPa]	0.0178	0.0556
ρ_m^0	Mobile dislocation density [m^{-2}]	$1x10^{12}$	$1x10^{12}$	$\rho_{ss,drx}$	Dislocation density in fully recrystallized material [m^{-2}]	-	$1x10^{14}$

[a] Parameter is calculated with CCT and TTT diagrams generated by JMatPro software based on the experiments.

References

1. Vedani M, Ripamonti D, Mannucci A, Dellasega D. Hot ductility of microalloyed steels. Metall Ital. 2008;100(5):19–24.
2. Gontijo M, Hoflehner C, Estermann P, Ilie S, Six J, Sommitsch C. Effect of Strain Rate on the Hot Ductility Behavior of a Continuously Cast Ti–Nb Microalloyed Steel. Steel Res Int. 2020;91(12).
3. Mintz B. Influence of composition on the hot ductility of steels and to the problem of transverse cracking. ISIJ Int. 1999;39(9):833–55.
4. Banks KM, Tuling A, Mintz B. Influence of thermal history on hot ductility of steel and its relationship to the problem of cracking in continuous casting. Mater Sci Technol. 2012;28(5):536–42.
5. T. N. Baker. Microalloyed steels [Internet]. Vol. 43, Ironmaking & Steelmaking Processes, Products and Applications. Informa UK Limited, trading as Taylor & Francis Group; 2016. 264–307 p. Available from: https://doi.org/10.1179/1743281215Y.0000000063.
6. Zheng Y, Shen W, Zhu L, Guo Z, Wang Q, Feng J, et al. Effects of composition and strain rate on hot ductility of Cr-Mo-alloy steel in the two-phase region. High Temp Mater Process. 2021;40(1):228–40.
7. Gontijo M, Hoflehner C, Ilie S, Six J, Sommitsch C. Comparison of hot ductility behavior of microalloyed steels with different B-, Cr-, Ni- and Ti-content. Met 2021 - 30th Anniv Int Conf Metall Mater Conf Proc. 2021;385–90.
8. Mintz B, Crowther DN. Hot ductility of steels and its relationship to the problem of transverse cracking in continuous casting. Int Mater Rev. 2010;55(3):168–96.
9. Hoflehner C, Ilie S, Six J, Beal C, Sommitsch C. Influence of Thermal History on the Hot Ductility of a Continuously Cast Low Alloyed Cr-Mo Steel. J Mater Eng Perform [Internet]. 2018;27(10):5124–9. Available from: https://doi.org/10.1007/s11665-018-3599-9.
10. Arıkan MM. Hot ductility behavior of a peritectic steel during continuous casting. Metals (Basel). 2015;5(2):986–99.
11. Kalidindi SR. Modeling the strain hardening response of low SFE FCC alloys. Int J Plast. 1998;14(12):1265–77.
12. Mirzadeh H, Cabrera JM, Najafizadeh A. Constitutive relationships for hot deformation of austenite. Acta Mater [Internet]. 2011;59(16):6441–8. Available from: http://dx.doi.org/10.1016/j.actamat.2011.07.008.
13. Zhong X ting, HUANG L ke, WANG L, LIU F, DONG X ming, ZHANG Z hua. A discontinuous dynamic recrystallization model incorporating characteristics of initial microstructure. Trans Nonferrous Met Soc China (English Ed [Internet]. 2018;28(11):2294–306. Available from: http://dx.doi.org/10.1016/S1003-6326(18)64874-5.
14. Kocks UF, Mecking H. Physics and phenomenology of strain hardening: the FCC case. Prog Mater Sci. 2003;48:171–273.
15. Zurob HS, Hutchinson CR, Brechet Y, Purdy G. Modeling recrystallization of microalloyed austenite: Effect of coupling recovery, precipitation and recrystallization. Acta Mater. 2002;50(12):3077–94.
16. Timoshenkov A, Warczok P, Albu M, Klarner J, Kozeschnik E, Bureau R, et al. Modelling the dynamic recrystallization in C-Mn micro-alloyed steel during thermo-mechanical treatment using cellular automata. Comput Mater Sci [Internet]. 2014;94(C):85–94. Available from: http://dx.doi.org/10.1016/j.commatsci.2014.02.017.

17. Huang K, Logé RE. A review of dynamic recrystallization phenomena in metallic materials. Mater Des [Internet]. 2016;111:548–74. Available from: http://dx.doi.org/10.1016/j.matdes.2016.09.012.
18. Humphreys FJ, Hatherly M. Recrystallization and Related Annealing Phenomena. Recrystallization and related annealing phenomena. 1963.
19. Kumar D, Kumar S, Nath SK. Study on hot deformation behavior of high carbon low alloy steel by constitutive and ann modeling and development of processing maps. Mater Perform Charact. 2020;9(2).
20. Bouaziz O, Buessler P. Mechanical behaviour of multiphase materials: An intermediate mixture law without fitting parameter. Rev Metall Cah D'Informations Tech. 2002;99(1).
21. Cabibbo M, Fabrizi A, Merlin M, Garagnani GL. Effect of thermo-mechanical treatments on the microstructure of micro-alloyed low-carbon steels. J Mater Sci. 2008;43(21):6857–65.
22. Mirzadeh H, Cabrera JM, Prado JM, Najafizadeh A. Hot deformation behavior of a medium carbon microalloyed steel. Mater Sci Eng A [Internet]. 2011;528(10–11):3876–82. Available from: http://dx.doi.org/10.1016/j.msea.2011.01.098.
23. Belyakov A, Miura H, Sakai T. Dynamic recrystallization under warm deformation of a 304 type austenitic stainless steel. Mater Sci Eng A. 1998;255(1–2):139–47.
24. Sakai T, Belyakov A, Kaibyshev R, Miura H, Jonas JJ. Dynamic and post-dynamic recrystallization under hot, cold and severe plastic deformation conditions. Prog Mater Sci. 2014;60(1):130–207.